J Neurophysiol 121: 2364–2378, 2019.
First published April 17, 2019; doi:10.1152/jn.00496.2018.

RESEARCH ARTICLE | *50 Years of Modeling Neural Activity: Celebrating Jack Cowan's Career*

Visual cortex neurons phase-lock selectively to subsets of LFP oscillations

N. V. Swindale[1] and M. A. Spacek[2]
[1]*Department of Ophthalmology and Visual Sciences, University of British Columbia, Vancouver, British Columbia, Canada; and* [2]*Division of Neurobiology, Department of Biology II, LMU München, Planegg-Martinsried, Germany*

Submitted 24 July 2018; accepted in final form 12 April 2019

Swindale NV, Spacek MA. Visual cortex neurons phase-lock selectively to subsets of LFP oscillations. *J Neurophysiol* 121: 2364–2378, 2019. First published April 17, 2019; doi:10.1152/jn.00496.2018.—It is generally thought that apart from receptive field differences, such as preferred orientation and spatial frequency selectivity, primary visual cortex neurons are functionally similar to each other. However, the genetic diversity of cortical neurons plus the existence of inputs additional to those required to explain known receptive field properties might suggest otherwise. Here we report the existence of desynchronized states in anesthetized cat area 17 lasting up to 45 min, characterized by variable narrow-band local field potential (LFP) oscillations in the range 2–100 Hz and the absence of a synchronized 1/*f* frequency spectrum. During these periods, spontaneously active neurons phase-locked to variable subsets of LFP oscillations. Individual neurons often ignored frequencies that others phase-locked to. We suggest that these desynchronized periods may correspond to REM sleep-like episodes occurring under anesthesia. Frequency-selective codes may be used for signaling during these periods. Hence frequency-selective combination and frequency-labeled pathways may represent a previously unsuspected dimension of cortical organization.

NEW & NOTEWORTHY We investigated spontaneous neuronal firing during periods of desynchronized local field potential (LFP) activity, resembling REM sleep, in anesthetized cats. During these periods, neurons synchronized their spikes to specific phases of multiple LFP frequency components, with some neurons ignoring frequencies that others were synchronized to. Some neurons fired at phase alignments of frequency pairs, thereby acting as phase coincidence detectors. These results suggest that internal brain signaling may use frequency combination codes to generate temporally structured spike trains.

local field potential; neural synchrony; oscillations; phase-locking; visual cortex

INTRODUCTION

The significant forms of functional variation among neurons in primary visual cortex include properties that can be established by measuring responses to visual stimuli, such as preferred orientation, eye and spatial frequency preference, and whether the receptive field type is simple or complex (Hubel and Wiesel 1962). Cells have additionally been characterized as excitatory or inhibitory on the basis of their spiking frequency and spike shape (Barthó et al. 2004). Cells have also been typed on the basis of responses to injected currents including bursting, chattering, and nonchattering classes (Nowak et al. 2003). However, this rather limited list obtained by analyzing spike train data is arguably at odds with the anatomical and biochemical complexity of the cortex (Ascoli et al. 2008; Kubota 2014; Stevens 1998), with the likely existence of >40 genetically distinct neuronal cell types (Tasic et al. 2016; Zeisel et al. 2015), and with the large number of inputs to cortical neurons that come from nongeniculate sources and that do not seem necessary to explain the physiological variation among cells that is seen. Hence it may be informative to search for physiological properties related to spiking behavior, additional to those derived from visual stimulation, that point to functional differences between cells.

In this article we report results from experiments in which we recorded spontaneous activity from neurons in anesthetized cat visual cortex (area 17) with multielectrode array electrodes. These experiments were done along with others in which we measured responses to a variety of types of visual stimuli. During the experiments we noticed the existence of alternating state changes in the local field potential (LFP) lasting many minutes. The most common state was a synchronous 1/*f* spectrum, which is the one normally observed under anesthesia and is thought to represent a state corresponding to slow-wave sleep (Harris and Thiele 2011; Tung and Mendelson 2004). However, we also observed states characterized by an absence of energy at low frequencies and the presence of variable frequency peaks including peaks in the theta, beta, and gamma ranges (Fig. 1). These desynchronized, oscillatory periods were unpredictable in length but could last 30 min or more. Similar transitions have been seen in recordings from anesthetized rat cortex (Clement et al. 2008) and were identified by these authors, on the basis of a variety of physiological criteria, as likely to correspond to rapid eye movement (REM) sleep states. In our recordings we found that responses to visual stimuli were noisier and less reliable during these desynchronized periods (Spacek and Swindale 2016). In the experiments reported here we measured the degree of synchrony between a neuron's spikes and the phases of particular desynchronized LFP frequency components by calculating spike-triggered LFP averages and examining the frequency components of these

Address for reprint requests and other correspondence: N. V. Swindale, Dept. of Ophthalmology and Visual Sciences, Univ. of British Columbia, 2550 Willow St., Vancouver, BC, Canada V5Z 3N9 (e-mail: swindale@mail.ubc.ca).

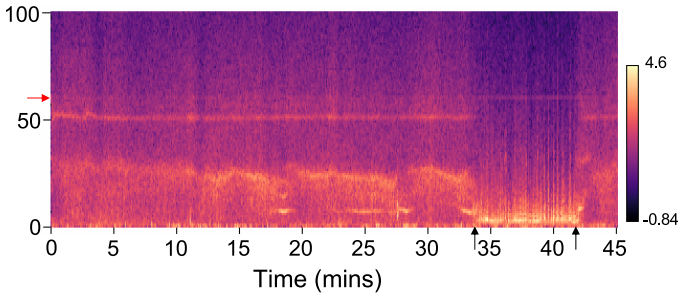

Fig. 1. The local field potential (LFP) frequency spectrum reveals brain state changes in anesthetized cats: LFP frequency spectrogram (log power in arbitrary units) of a 45-min period of spontaneous activity. Frequency (in Hz) is shown on the vertical axis. A desynchronized, oscillatory pattern of activity was present from 0 to 34 min, with dominant frequencies at around 8 (theta), 25 (beta), and 50 (gamma) Hz. At 34 min (1st black arrow) the LFP changed to a variable-amplitude synchronized 1/*f* pattern before reverting back at 42 min (2nd black arrow) to the desynchronized state. Red arrow shows a weak 60-Hz artifact. Key shows the mapping between log spectral power and color.

averages. We found that many neurons, though not all, showed highly selective, idiosyncratic patterns of phase-locking to subsets of LFP oscillations. Many neurons synchronized to more than one frequency and timed their spikes to specific phase combinations of frequency pairs. Individual neurons were specific in terms of which frequencies they synchronized to, ignoring some frequencies present in the LFP but responding to others. Because these results were obtained from neurons that were physically close to each other (<1 mm), they suggest the possibility that, in addition to the more familiar dimensions of orientation, ocular dominance, and spatial frequency, visual cortical neurons can be distinguished from each other in terms of frequency and frequency combination codes that are made manifest during desynchronized, REM sleep-like episodes.

METHODS

Experimental procedures. Experimental procedures were carried out in accordance with guidelines established by the Canadian Council on Animal Care and institutional protocols reviewed and approved by the Animal Care Committee of the University of British Columbia. Recordings were made in the visual cortex of cats anesthetized either with 0.5–1.5% isoflurane and 70% N_2O + 30% O_2 (*animal IDs ptc17*, *ptc18*, and *ptc22*) or with continuously infused propofol (6–9 $mg \cdot kg^{-1} \cdot h^{-1}$) and fentanyl (4–6 $\mu g \cdot kg^{-1} \cdot h^{-1}$) (*ptc20* and *ptc21*). *Animals ptc17*, *ptc18*, and *ptc21* were male, and *ptc20* and *ptc22* were female. Heart rate and blood oxygenation were monitored with a pulse oximeter (Nonin 8600V). Mean arterial blood pressure was monitored with a Doppler blood pressure monitor (Parks Medical 811-B) placed on a shaved section of hind leg. Body temperature was maintained at 37°C with a homeothermic blanket (Harvard Apparatus). Eye movements were prevented either by continuous infusion of pancuronium bromide (*ptc20*, *ptc21*, and *ptc22*) or by retrobulbar injections of α-bungarotoxin (Tocris) (*ptc17* and *ptc18*). Pupils were dilated with tropicamide (0.5%). The eyes were refracted to a viewing distance of 57 cm with rigid gas-permeable contact lenses. A craniotomy was made, the dura removed, and a nick made in the pia with an ophthalmic slit knife. The electrode array was then inserted perpendicularly into the cortex under visual control so that the upper channels lay ~100–200 μm below the surface. The craniotomy was filled with agarose gel (2.5%, type III-A; Sigma-Aldrich, St. Louis, MO) in artificial cerebrospinal fluid at 38–40°C. Recordings were made with 54-channel electrode arrays (University of Michigan Center for Neural Communication Technology and NeuroNexus). Arrays, diagrammed in Fig. 2, had single shanks with either two (*ptc18*, *ptc20*, and *ptc21*) or three (*ptc17* and *ptc22*) columns of channels. Channels were 15 μm in diameter and made of iridium. Voltage signals were analog band-pass filtered between 500 Hz and 6 kHz, sampled at a rate of 25 kHz, and digitized with 12-bit resolution (Blanche et al. 2005). Low-pass LFP recordings were obtained from 10 of the 54 channels fed in parallel to a separate set of amplifiers. They were analog band-pass filtered between 0.1 and 150 Hz and sampled at a rate of 1 kHz with 12-bit resolution. These channels were numbered sequentially from 1 to 10, starting at the top of the electrode. On the three-column electrodes the channels were 128 μm apart, with the exception of *channels 9* and *10*, which were 64 μm apart (*ptc17* and *ptc22*). On the two-column electrodes the channels were 150 μm (*ptc18* and *ptc20*) or 195 μm (*ptc21*) apart, with *channels 9* and *10* being 100 μm (*ptc18* and *ptc20*) or 130 μm (*ptc21*) apart. These channels also provided, in parallel, a normal high-pass signal used for spike identification.

Data reported here were obtained from a total of 16 electrode penetration sites in 10 hemispheres of five adult cats. Recording sites were in area 17, and receptive fields were typically within 10° of the area centralis. For the purposes of this report the term "recording" is used to mean a single period of continuous data acquisition, typically lasting between 10 and 60 min. Several recordings might be made at a single recording site. Periods of spontaneous activity lasting from 5 to 60 (average = 27) min were recorded at each site. During these

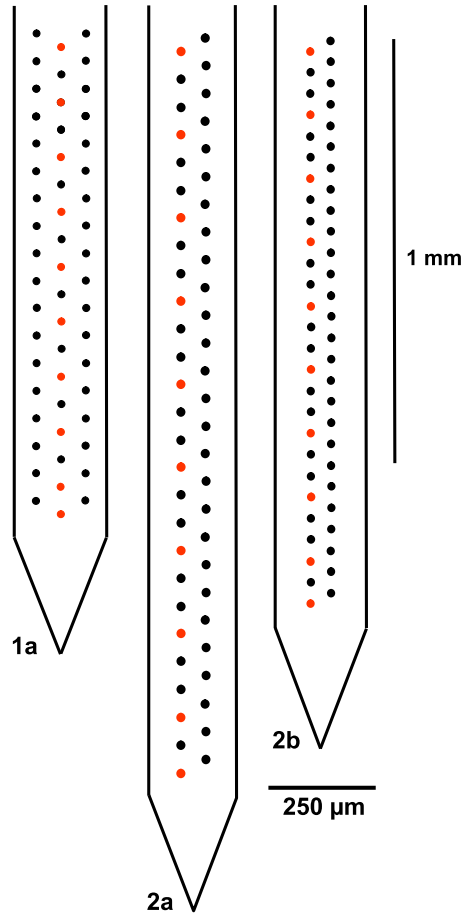

Fig. 2. Diagrams of the 3 types of multielectrode array used in the experiments, shown at the same scale. Red dots mark channels that fed both low (local field potential)- and high (spike)-pass signals to the amplifiers. Type 1a was used for *experiments ptc17* and *ptc22*, type 2a was used for *ptc21*, and type 2b was used for *ptc18* and *ptc20*. Channel spacing was 64 μm for type 1a, 65 μm for type 2a, and 50 μm for type 2b. Channels are shown at approximately the correct scale relative to their spacing.

periods the cat viewed, either binocularly or monocularly through the dominant eye, through 3-mm artificial pupils, a field of uniform luminance (58 cd/m^2) on a CRT monitor (Iiyama HM903DTB) with a refresh rate of 200 Hz, positioned 57 cm from the eyes. An additional six periods of recording of 16- to 20-min duration during periods of desynchronized activity were made in three animals viewing uniform luminance with the screen refresh rate set at 66 Hz. Experiments on a single animal lasted up to 3 days before euthanasia.

Visual stimuli used in other experiments, not reported here, included white noise (m sequence) stimuli, moving bars, sine wave gratings, and natural scene movies. At each site, typically 20–60 units were isolated, off-line, with sorting methods described in Swindale and Spacek (2014). The position of the unit on the electrode array was estimated during spike sorting as the peak-to-peak weighted average of the positions of the channels (typically 5–10 in number) on which the averaged spike waveform exceeded a fixed threshold. Units were rejected for inclusion if their signal-to-noise ratio (defined as peak-to-peak height measured within a temporal window of −0.4 ms to 0.6 ms divided by the root mean square value of the voltage signals measured on either side of the window) was <1.5.

Data selection. Not all of the recordings contained periods of desynchronized, oscillatory, LFP activity, although many did. For the purposes of quantifying the relations between unit spiking activity and the LFP record we chose a subset of nine recordings of spontaneous activity from the complete set, each lasting between 16 and 45 min, with only a single recording from each electrode penetration. When more than one recording was made at a single site we chose the recording with the longer duration. All of the recordings were considered to show desynchronized LFP activity, as judged by a relative lack of energy at frequencies below 5 Hz and by the presence of narrow-band energy in the LFP frequency spectra. A period of synchronized activity in one recording (shown in Fig. 1) was masked from analysis. These nine recordings included at least one recording from each of the five animals.

Electrode depth. In most cases (6/9) the electrode was placed so that the uppermost channel lay just below the surface of the cortex, as judged visually during insertion. In three other cases the electrode had been moved further below the cortex, by distances of between 300 μm and 600 μm, before recording. In all cases the insertion position was close to the crown of the gyrus and the insertion angle was judged visually to be close to perpendicular to the surface. In postexperiment histological reconstruction of the electrode tracks it proved hard to determine the exact position of the electrode, perhaps because the electrodes are extremely thin and did not leave easily visible signs of damage. In penetrations where the top of the electrode lay just below the cortical surface it would be safe to assume that the upper part of the recording came from the upper cortical layers; however, the location of layer IV and the subgranular layers would be uncertain.

Experimental design and statistical analysis. In what follows, quantities measured in the time domain are mainly denoted by lowercase symbols, while uppercase symbols are mostly used for quantities measured in the frequency domain. For example, $V(f)$ is the Fourier spectrum of the voltage signal $v(t)$.

The LFP power spectrum, $V_l(f)$, was calculated as the sum of the power spectra of half-overlapping, windowed segments of the voltage record:

$$V_l(f) = \frac{1}{M}\sum_{m=1}^{m=M} \left|\Im\{v_l(t+t_m)h(t)\}\right|^2 \quad (1)$$

where f is frequency, l is the LFP channel number (1–10), m indexes the segments, M is the total number of segments, $\Im()$ denotes Fourier transformation, $|\ |$ denotes the magnitude of the complex argument, $v_l(t + t_m)$ is the LFP voltage on channel l at time sample point $(t + t_m)$, and $h(t)$ is a windowing function. Fourier transforms used a 2,048-point fast Fourier transform (FFT) with a Bartlett window, i.e., $h(t) = 1 - \left|\frac{t}{w}\right|$ and $w = 1{,}024$, $t_m = 1{,}024m + 1$, and M determined by the duration of the recording.

To measure synchrony between the times at which spikes occurred and the phases of frequency components of the LFP, we first calculated the spike-triggered average, $c_l(t)$, of the LFP voltage, given by

$$c_l(t) = \frac{1}{N}\sum_{n=1}^{N} v_l(t_n + t) \quad (2)$$

where t_n is the time of the nth spike of the unit and N is the total number of spikes fired. The average was usually calculated for $-1{,}023 < t < 1{,}024$ ms. (Because the LFP sample frequency was 1 kHz there is 1 sample point per millisecond). We refer to $c_l(t)$ as the spike-triggered local field potential (ST-LFP) in what follows.

The power spectrum of the ST-LFP is given by

$$C_l(f) = \left|\Im\{c_l(t)\}\right|^2 \quad (3)$$

The amplitudes of frequencies in the ST-LFP spectrum are difficult to interpret statistically. Note that the amplitude of a particular ST-LFP frequency component is the vector sum of individual frequency components, one for each spike. Each of these is a two-dimensional vector corresponding to the real and imaginary parts (or equivalently the phase angle and length) of the LFP waveform at a given frequency and the time of the spike. These sum to give a resultant whose length (or length squared in the case of a power spectrum) determines the amplitude of the ST-LFP power spectrum. A common approach to analyzing sums of oriented vectors (e.g., Fisher 1993) is to compute a normalized vector length measure, which is the length of the resultant divided by the sum of the lengths of the individual vectors. This measure is bounded by 0 and 1: it will equal 1 if all the vectors have an identical phase angle. A vector sum of random phases (as in a random walk) does not have an expected length of 0, however. This measure, here termed the normalized ST-LFP spectrum, is

$$Q_l(f) = \frac{\left|\sum_{n=1}^{N} \Im\{v_l(t+t_n)h(t)\}\right|}{\sum_{n=1}^{N} \left|\Im\{v_l(t+t_n)h(t)\}\right|} \quad (4)$$

Q is determined by the distribution of phase angles as well as the lengths of the individual vectors. Subject to the above qualifications it can also be regarded as measuring an effect size, which can be taken into consideration along with the statistical tests of significance described next. The aim of the present study was to test the hypothesis that the phase angles are not random. If the lengths are all the same, the statistics of the resulting net length distribution for random phases are easy to determine (e.g., Jeans 1967). However, in the present case the net length and the resulting statistics depend on both the distribution of phase angles and the lengths. As an example of how the length distribution can complicate the interpretation, consider the case in which the majority of the vectors have a small length and random phases together with a small number of very long vectors. The net length distribution will be dominated by the behavior of these few vectors, and statistical tests will have limited power. To circumvent this difficulty we simply tested the null hypothesis that the distribution of phase angles, independent of length, was unimodally different from uniform, with an unspecified mean direction, using the Rayleigh z statistic (Fisher 1993). This test lacks some power because lengths are ignored; however, in most cases the resulting P values for frequency peaks in the spike-triggered LFP power spectrum were highly significant. Because large numbers of tests were performed (1 for each frequency and channel) a Bonferroni correction was applied when using significance levels to identify peaks.

We additionally calculated the ST-LFP power spectrum, which is the sum of the power spectra of segments of the LFP waveform, each centered on a spike. Hence it represents the power spectrum that was present when the unit in question fired spikes. Unlike $C_l(f)$, its amplitude is not dependent on phase alignments because the power, which is phase insensitive, is calculated before the spike-triggered sections are added. Its value is given by

$$S_l(f) = \frac{1}{N}\sum_{n=1}^{N} \left|\Im\{v_l(t+t_n)h(t)\}\right|^2 \quad (5)$$

Note that if spikes fire independently of LFP frequency amplitudes, this measure will approximate the LFP power spectrum. Hence a measure of the dependence of firing on LFP frequency amplitudes, independent of any phase alignment, here termed spike-power coherence, is given by

$$P_l(f) = \frac{S_l(f)}{V_l(f)} \quad (6)$$

This measures the relationship between a unit's firing rate, measured in ~2-s periods, and the presence or absence of LFP energy in a particular frequency band. If there is no relationship $P(f) \approx 1$, values > 1 indicate that the unit was more likely to fire during periods of higher than normal energy in the frequency band concerned, and values < 1 indicate that the unit was less likely to fire.

Peaks in the ST-LFP power spectrum were identified by first smoothing $C_l(f)$ with a Gaussian of width $\sigma = 5.0$ Hz in the frequency domain and $\sigma =$ (distance between LFP channels) in the channel (spatial) domain. A peak was counted if all of the following were true: *1*) it was a local maximum after smoothing; *2*) the Bonferroni-corrected ($n =$ the number of frequencies tested $\times$ the number of channels) P value derived from the Rayleigh phase angle test was <0.001; *3*) the frequency was within the range 2–100 Hz; and *4*) the amplitude of $C_l(f) > 5.0$. The latter criterion was applied to remove very low-amplitude peaks that sometimes occurred at frequencies $>$ 60 Hz. Note that these criteria are conservative and it is likely that some excluded candidate peaks were also statistically significant. A similar procedure was used to identify "probe" peaks in the LFP power spectrum. These were used to test for the absence of statistically significant phase-locking of specific units to particular frequency peaks present in the LFP. In this case artifactual peaks at a frequency of 60 $\pm$ 0.5 Hz that were present in some recordings were excluded. No other exclusion criteria were applied.

Control conditions, described in more detail below, included the following tests: *1*) spike times were individually jittered by a defined random amount; *2*) the spike train was shifted by adding a single fixed positive or negative time to that of each spike (hence preserving the intervals between spikes); or *3*) the entire LFP signal was time reversed. The accuracy of the frequency measurements was tested by replacing the biological LFP signal with sine waves of known frequencies and then repeating the estimates of peak frequency. The difference between these estimates and the known frequencies averaged -0.006 ± 0.15 Hz ($n = 38$ frequencies evenly spaced between 5 and 97.5 Hz), with no error > 0.25 Hz.

To examine whether individual spikes tend to fire preferentially at specific phase combinations of different frequencies, we calculated histograms, $J(i, j)$, of the distribution of phase angles, ϕ_1 and ϕ_2, with binned values i and j, respectively, of individual spikes, for pairs of frequency peaks identified in the ST-LFP spectrum. For each unit, we identified pairs of frequency peaks in the ST-LFP and their peak channels. For each spike, we calculated the Fourier transform of a single 2,048-point sample of the LFP, centered on the spike. We then measured the phase values for the two frequencies on the respective channels, binned them using 18°-wide bins, and incremented the corresponding histogram value $J(i, j)$. Tests were conducted on frequency pairs in units that satisfied all of the following criteria: *1*) there were >1,000 spikes; *2*) there were two or more significant frequency peaks in the ST-LFP spectra; and *3*) their frequency ratios (higher to lower) were not close to integer values, i.e., within any of the ranges 1.0–1.2, 1.8–2.2, or 2.8–3.2. This was done to avoid rare examples of harmonic frequency relationships (leading to easily identified relationships such as $\phi_1 = 2\phi_2$). For units where there were more than two qualifying peaks, all combinations of frequency pairs were tested. This yielded a total of 69 pairs, including examples from eight of the nine recordings. We also calculated control distributions obtained by time-reversing the LFP recording data.

The joint-phase distributions were further characterized by doing a least-squares fit to $J(i, j)$ of a model two-dimensional bell-shaped distribution, $M(i, j)$ given by the product of two von Mises functions (Batschelet 1981):

$$M(i,j) = A\exp\{k_i[\cos(\phi_i - \phi_{i\max}) - 1]\} \times \exp\{k_j[\cos(\phi_j - \phi_{j\max}) - 1]\} \quad (7)$$

where A is the maximum height, $\phi_i = \frac{\pi(i-1)}{10}$, $\phi_j = \frac{\pi(j-1)}{10}$, k_i and k_j are width parameters, and $\phi_{i\max}$ and $\phi_{i\max}$ are the peak phases for i and j, respectively. Levenburg-Marquardt optimization (Press et al. 1994) was used to do the fitting. The width of the peak was quantified as the distance (measured in degrees of phase angle) to half-height from the fitted function, taken along the diagonal. This width is given by $w = \cos^{-1}[\log_e(0.5) + k_i + k_j]/(k_i + k_j)$.

RESULTS

Steps involved in calculating the ST-LFP power spectrum. Figure 3 illustrates the steps involved in the calculation of the ST-LFP and its power spectrum. Figure 3*A* shows superimposed LFP records aligned to the times of 10 randomly chosen spikes and illustrates the fact that the extracted averaged signals, typically obtained from several thousand spikes, were about an order of magnitude smaller than the raw LFP signals (the solid red line in Fig. 3*A* is the average of 16,605 spikes). Figure 3*B* shows this averaged signal from one neuron in more detail. A large negative dip is present, preceded and followed by oscillatory ripples. A similar relationship between the occurrence of spikes and a negative dip in the LFP has been noted by other researchers (e.g., Destexhe et al. 1999; Nauhaus et al. 2009). In Fig. 3, *C* and *D*, and subsequent figures, signals from the 10 LFP channels are displayed with a gray scale for voltage or spectral power and are arranged vertically, with *channel 1* at the top and *channel 10* at the bottom. Channels span the length of the electrode array. The position of the recorded unit relative to the electrode is normally shown as a red dot on the left of the panel. Figure 3*C* shows one such complete set of spike-triggered averaged LFP signals displayed with this convention, with a time window of $\pm$250 ms. In this particular recording there was a strong effect of depth on the timing (or phase) of the negative dip, with the phase appearing to reverse across the middle cortical layers. A consistent relation between phase and depth was not observed in all the recordings, however, and we have not attempted to analyze it further. Figure 3*D* shows the power spectrum derived from the ST-LFP waveforms, using a temporal window of $\pm$1,024 ms, with frequency peaks at around 7, 24, and 51 Hz. Red dots indicate the positions of statistically significant (corrected $P < 0.001$) frequency peaks, identified with the Rayleigh test for nonrandom phase angles, as described in METHODS. Because frequency peaks $>$ 70 Hz were uncommon, frequencies above this are not shown on the

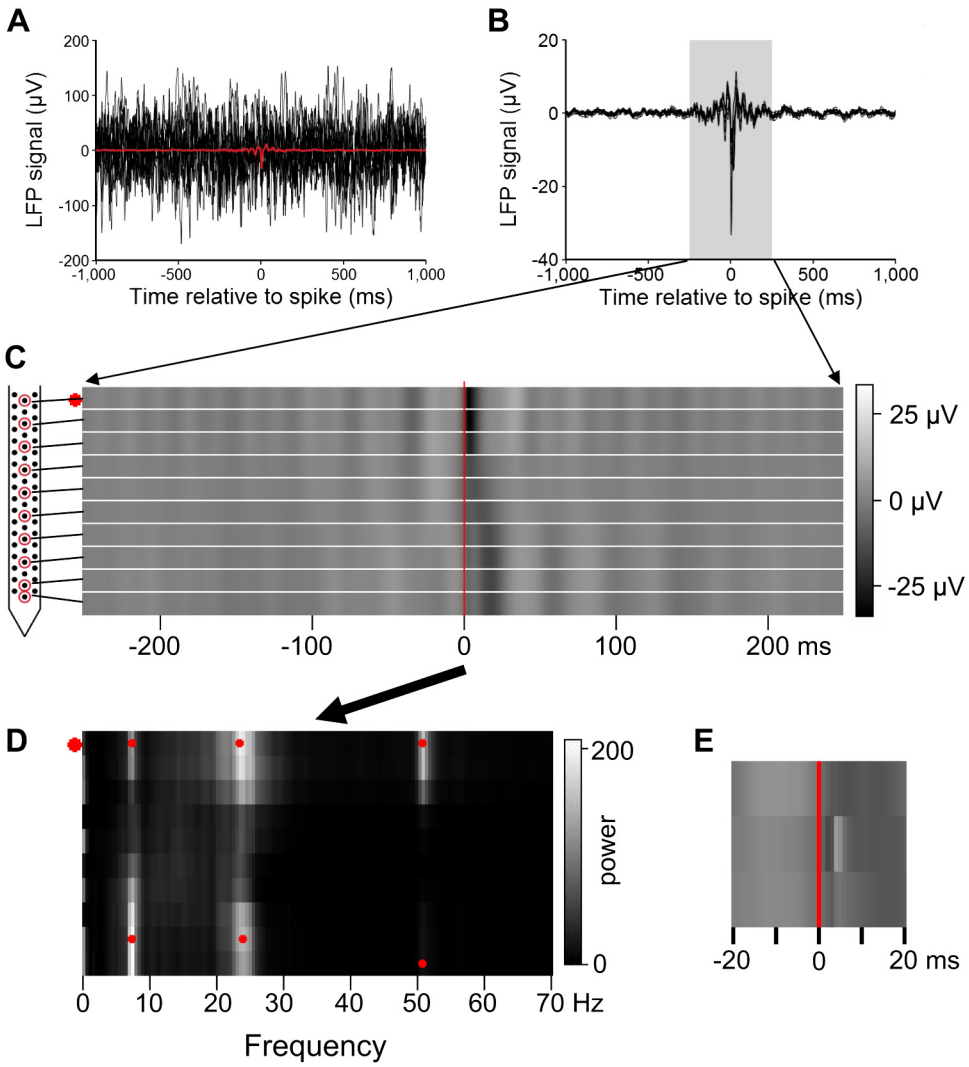

Fig. 3. Steps involved in calculating the spike-triggered local field potential (ST-LFP) power spectrum. *A*: superposition of LFP waveforms (black traces) from a single electrode channel (*channel 1*), each centered on 1 of 10 randomly chosen spikes from a particular unit. The continuous red line shows the average LFP waveform triggered by all ~17,000 spikes fired by the unit during the periods of synchronized activity shown in Fig. 1. *B*: superimposed averaged ST-LFP traces from each of the 10 LFP channels. Another way of displaying the same data is shown in *C*. Here the voltages are displayed with a gray scale (as indicated by the key), and the traces from the LFP channels are stacked vertically in an order that corresponds to the vertical order on the recording electrode (red circles around the channels shown in electrode diagram on *left*). Hence vertical position on the diagram corresponds to position on the electrode and cortical depth. The same convention of arranging the 10 LFP channels vertically is used in subsequent figures. *D*: power spectra obtained from 2,048-point Fourier transforms of the 10 averaged traces shown in *C*. The small red dots in *D* show the positions of statistically significant frequency peaks, identified as described in METHODS. The larger red dots shown on *left* in *C* and *D* show the position of the recorded unit relative to the LFP channel positions. This convention is also used in subsequent figures. *E*: a section of ST-LFP waveform on a subset of 3 adjacent LFP channels with an expanded timescale showing a localized spike signature in the averaged LFP waveform. The signature is delayed by ~3 ms, indicating a timing delay in the LFP, presumably resulting from hardware filtering. The vertical red lines in *C* and *E* indicate $t = 0$.

spectral plots. Because the ST-LFP signal decays to near zero, typically within ±250 ms, and hence is naturally windowed, the particular choice of a temporal window of ±1,024 ms for the power spectral calculation is unlikely to have much effect, i.e., a longer or slightly shorter window would be expected to have little effect on the spectrum.

Spikes contribute directly to LFP signals. Figure 3*E* illustrates a phenomenon that was observed in ~20% of units. A very brief voltage inflection in the average LFP waveform occurred ~2–3 ms after the spike, normally on only the channel that was closest to the estimated position of the unit. We interpret this as the residue of the extracellular spike signal and that the low-pass filtering used to remove frequencies higher than 150 Hz was incomplete. The presence of a small but detectable signal in the LFP resulting directly from the spikes of just one neuron suggests that there could be a significant contribution to the LFP resulting from all the active neurons in the close vicinity of a channel. Such contributions, being brief and to the extent they approximate delta functions, would be expected to contribute broadband energy to the overall frequency spectrum. Indeed, there was normally a high positive correlation between the summed firing rate of all the units and LFP spectral activity summed over frequency ranges of 50–100 Hz that included no peaks. This was true in both synchronized and desynchronized states. At least some of this correlation could be due to very local spike signals from neurons contributing broadband power to the LFP.

Some units synchronize to specific LFP frequencies; others do not. Figure 4 shows patterns of ST-LFP waveforms in 10 simultaneously recorded units, chosen (on the basis of the power spectra) to illustrate variability across neurons. This variability is much more evident in the corresponding power spectra (Fig. 5). The oscillation frequencies to which units showed synchrony were always a subset of those present in the LFP, but the particular subset varied distinctively from cell to cell. For example, among the 10 units shown, statistically significant ST-LFP synchrony at ~7 Hz was present in *units 1*, *4*, *19*, and *42* but not in the remainder; synchrony at 23 Hz was present in all units except *unit 71*; synchrony to a 14-Hz component on the middle channels was present only in *units 52* and *76*; synchrony with a 51-Hz component on the upper channels was present in *units 1*, *4*, *52*, *71*, and *76*. There was no clear relationship between the position of a unit and the frequency pattern to which it synchronized. Beyond the localized signal illustrated in Fig. 3*E*, it was not possible to deduce the position of a cell from the distribution of ST-LFP amplitudes along the length of the electrode.

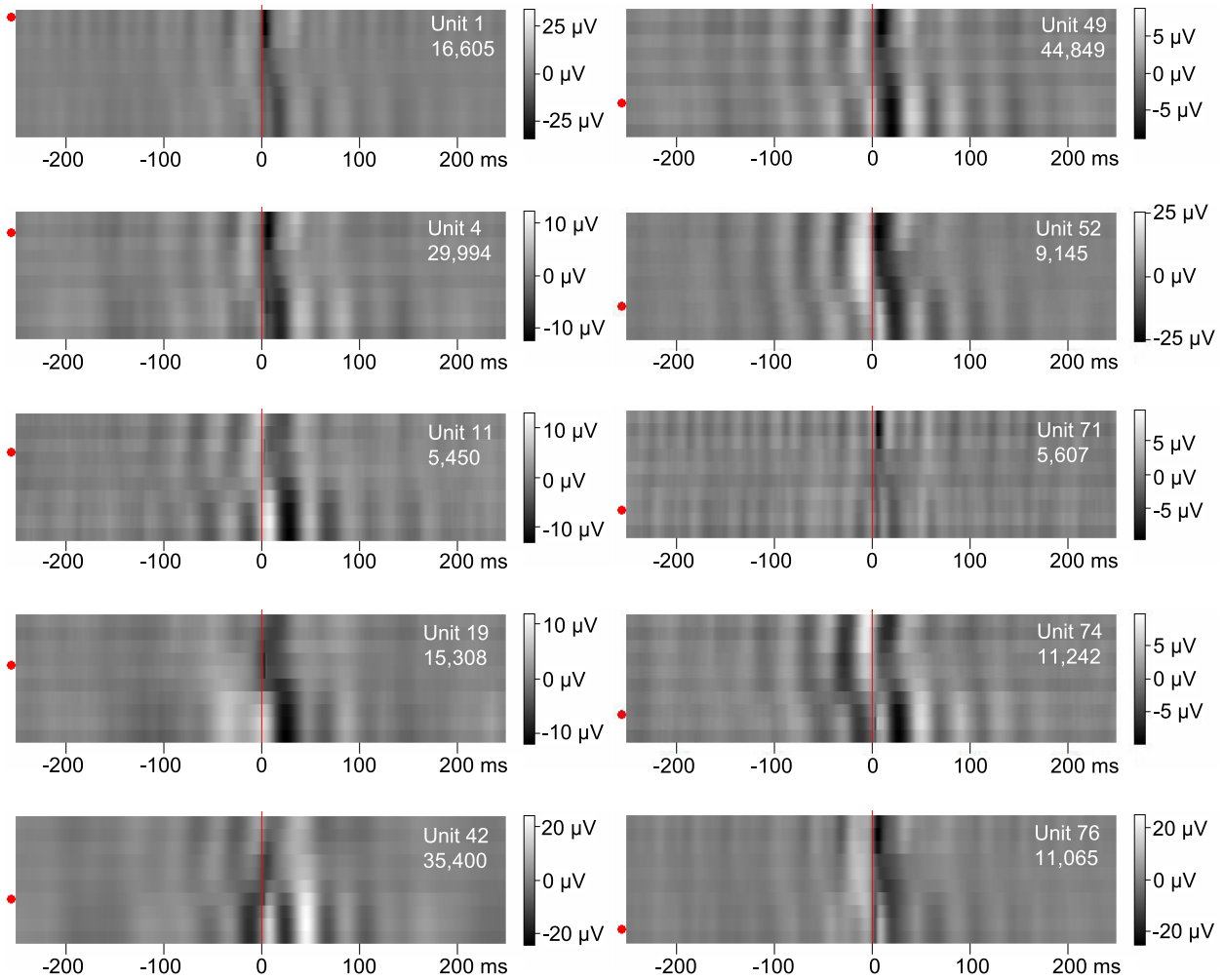

Fig. 4. Spike-triggered local field potential waveforms from 10 simultaneously recorded units. Examples were selected from a total of 86 units. *Top left* panel (*unit 1*) is also shown in Fig. 3*C*. The display convention in Fig. 3*C* is used here. The number of spikes on which each average is based is shown below the unit number.

It is possible that some of these differences may be due to the relatively conservative criteria used to identify peaks and that most units showed some degree of synchrony to the same set of frequencies and LFP channel locations. The remaining degree of variability might result from other variable factors, perhaps causing cells not to fire at times when certain LFP frequencies were present and vice versa. It seemed, however, that many potential peaks were genuinely absent in some cells. Figure 6 shows the normalized vector length measure Q (*Eq. 4*) plotted as a function of frequency for five simultaneously recorded units, selected to illustrate differences. Note that Q also provides a measure of effect size, which although not straightforward to interpret directly (see METHODS) can be contrasted with the tests based purely on significance levels. All of these units fired substantial numbers of spikes (>5,000). The normalized vector length measure was used for this comparison because the length depends only on the degree of phase synchrony and not on the amount of power in the LFP at a particular frequency, which can be quite variable. One unit (*unit 85*) showed no synchrony at all to any frequency; only one unit showed synchrony at 51 Hz; three units showed synchrony at ~23 Hz whereas two others did not; *unit 11* showed a synchrony peak at 23 Hz but not at any other frequency. Only *unit 1* showed peaks at three different frequencies. To further test for the absence of phase-locking to frequencies that were present in the LFP we carried out Rayleigh significance tests for synchrony of particular units to specific probe peaks, one set for each of the nine recordings, defined by a channel and a frequency, identified in the LFP spectrum as described in METHODS. There was a wide spread of Rayleigh significance values among the unit-peak pairs, including both high (insignificant) and low (highly significant) P values. Out of a total of 909 pairs we found 265 pairs for which $P < 0.001$ and 208 pairs for which $P > 0.5$.

Comparison of the ST-LFP spectrum with the spike train spectrum. The spike train (firing rate) spectrum was calculated from the Fourier transform of the spike train autocorrelation function, using a 2,048-point transform and a Bartlett window. Comparison of this spectrum with that of the ST-LFP revealed a variety of relationships, some examples of which are shown in Fig. 7. In many cases, peaks in the ST-LFP spectrum did not have a corresponding match in the spike-rate (Fig. 7*A*, *top*, peak at 8 Hz; Fig. 7*A*, *middle*, peak at 30 Hz); in other cases peaks coincided (Fig. 7*A*, *top*, at 52 Hz; Fig. 7*A*, *bottom*, at 25 Hz and 47 Hz). In a few cases peaks coincided in frequency with a dip in the firing rate spectrum (Fig. 7*A*, *top*, peak at 23

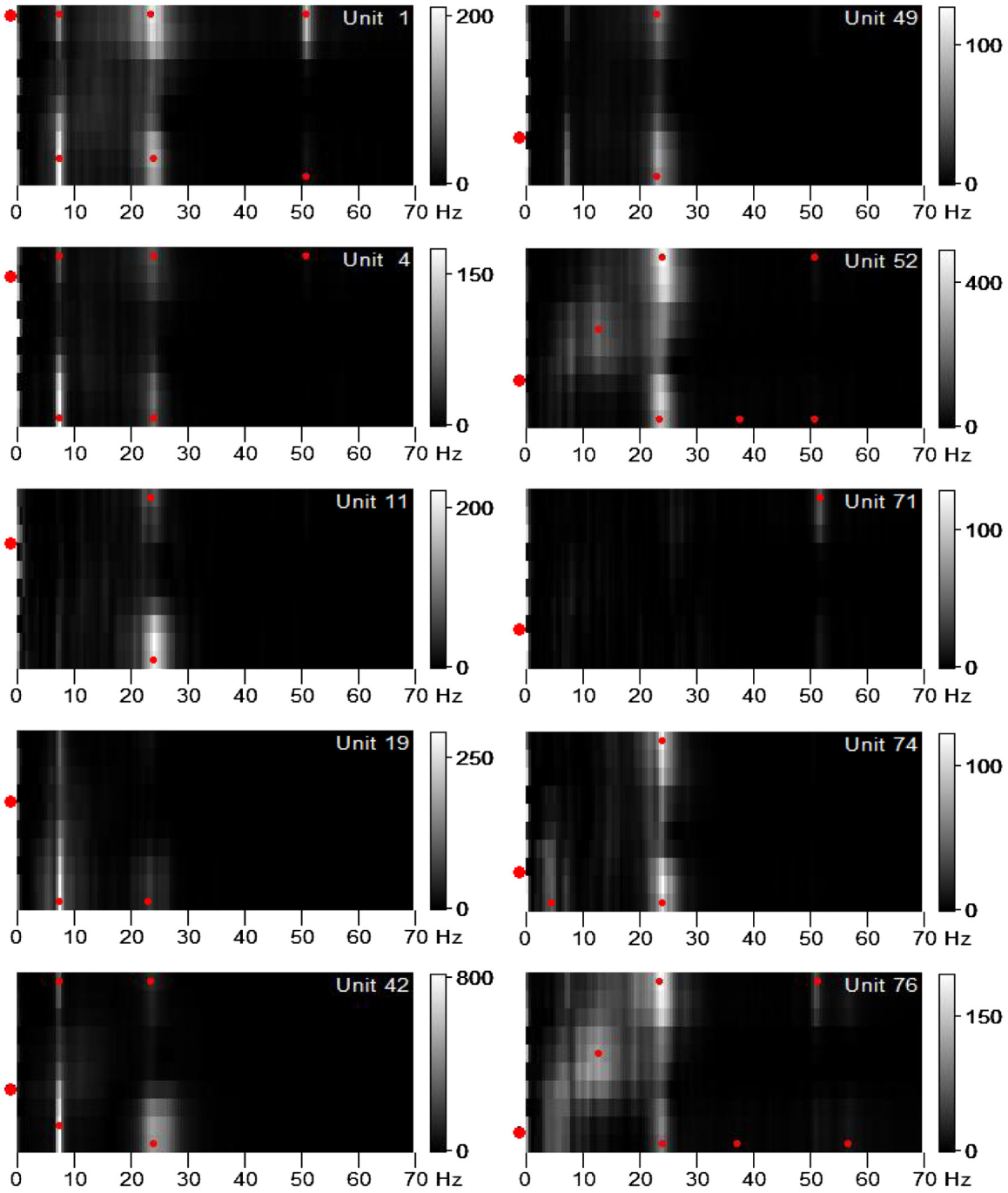

Fig. 5. Spike-triggered local field potential (ST-LFP) power spectra for the 10 units shown in Fig. 4. Spectra were calculated from Bartlett-windowed, 2,048-point fast Fourier transforms of the ST-LFP waveforms (*Eqs. 2* and *3*) and are displayed with a linear brightness scale. As in Fig. 3, the small red dots indicate statistically significant frequency peaks and the larger red dot at the side of each panel indicates the location of the recorded unit relative to the 10 LFP channels. The units shown were selected to demonstrate the variety of spectral signatures that can be seen across simultaneously recorded units.

Hz). The relationship between the peaks was further quantified by taking, for each peak in the ST-LFP spectrum, detected as described in METHODS, the central value and the four points in either side (so 9 points in all) and calculating the Pearson cross-correlation with the same nine frequency values in the spike-train power spectrum. Units with <1,000 spikes were omitted from the analysis. The resulting histogram of correlation values is shown in Fig. 7*B*. This suggests that the peak-unit pairs fell into two, roughly equal-sized, groups: those where there was a coincident peak in the firing rate spectrum (points with a correlation $r > 0.5$) and those where there was no relation or a negative one.

ST-LFP peak numbers vary across units. To further quantify the variation in peak numbers across units we plotted the total number of frequency peaks per unit, ignoring duplication of peaks at similar frequencies on different channels (which was common). Figure 8*A* plots the number of peaks per unit for all units ($n = 614$ units) in the sample of nine recordings as a function of the number of spikes fired. Figure 8*B* shows the distribution of the number of peaks across units. Although the

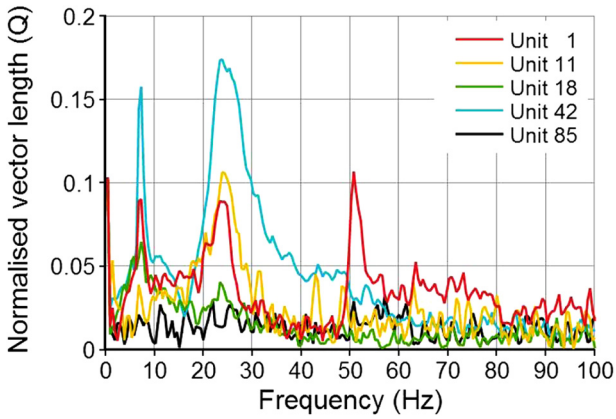

Fig. 6. Further evidence of highly variable synchrony across units: graphs of normalized vector length Q (*Eq. 4*) as a function of frequency for 5 different simultaneously recorded units, chosen to illustrate the varying presence and absence of synchrony in different units. All data come from the same local field potential channel. The number of spikes on which each average is based was *unit 1*: 16,605; *unit 11*: 5,450; *unit 18*: 24,976; *unit 42*: 35,400, and *unit 85*: 12,377.

majority of units (447/614) did not show significant phase-locking, a substantial percentage (167/614 = 27%) did. The number of spikes and the number of peaks were correlated (Spearman's rank correlation = 0.33, $P = 2 \times 10^{-12}$). The number of spikes was significantly lower for zero peaks compared with one peak ($P < 0.001$, Mann-Whitney U-test, $z = 4.55$) and for one peak compared with two peaks ($P < 0.001$, z = 3.83); however, differences between two and three peaks and between three and four peaks were not significant. It is possible that had the recordings continued for longer, so that more spikes were recorded, more of the units would have shown significant phase-locking to one or more frequencies. However, it is also possible that units are of two types: those that are capable of phase-locking and those that are not. A third possibility is that those units that did not phase-lock were insensitive to the particular frequencies that were present during the periods of recording and that at other times they would phase-lock to different frequencies.

We plotted the distribution of frequencies to which phase-locking was found. The frequencies fell roughly into three groups (Fig. 9*A*): *1*) 2–10 Hz, *2*) 20–35 Hz, and *3*) 45–70 Hz. These correspond approximately with the traditional theta, beta, and gamma bands (with 40 Hz notably absent). Although grouping into these bands might be expected, the data come from a limited set of animals and the particular frequencies with which synchrony was found were quite variable across individual recordings (Fig. 9*B*). Whether samples from additional recordings would reveal the same grouping is not certain. Other than the traditional use of nomenclature, the authors are not aware of evidence for discrete categories for brain frequencies, i.e., that certain frequency bands are avoided.

Synchrony is not related to slow changes in firing rate or spike-power coherence. The finding that cells differ in the frequency sets to which they synchronize might be explained as an incidental result of different cells firing at different times, these times coinciding systematically with the presence or absence of certain LFP frequencies at particular times. A positive temporal correlation between firing rate and energy at a particular frequency would not invalidate the statistical significance of the relation with phase, but the absence of such a relationship might be a consequence of a cell tending not to fire when a particular frequency was present. To test this we calculated, for each unit, the Pearson correlation between its firing rate, measured in 5.1-s intervals, and the power in the LFP for each LFP probe frequency and channel, measured in the same time intervals. LFP spectral power was calculated from half-overlapping 2,048-point FFTs, giving one sample per 1.024 s. Five consecutive samples were then added to give a single power value for a particular frequency in a 5.1-s window. Firing rate was given by the number of spikes occurring in the same time period. Units firing <500 spikes were excluded from the analysis. Figure 10*A* shows the distribution of correlation values for unit-frequency pairs where there was statistically significant phase-locking ($P < 0.001$, $n = 257$ pairs; Fig. 10*A*, *left*) and for pairs where there was no evidence for phase-locking ($P > 0.5$; $n = 169$ pairs; Fig. 10*A*, *right*). The distributions are similar. Figure 10*B* shows the corresponding distributions for the related spike-power coherence measure (*Eq. 6*). If the measure > 1 for a particular frequency then it means that, on average, LFP power at that frequency was that much greater than normal at the times when the cell fired; a measure < 1 correspondingly means that the cell

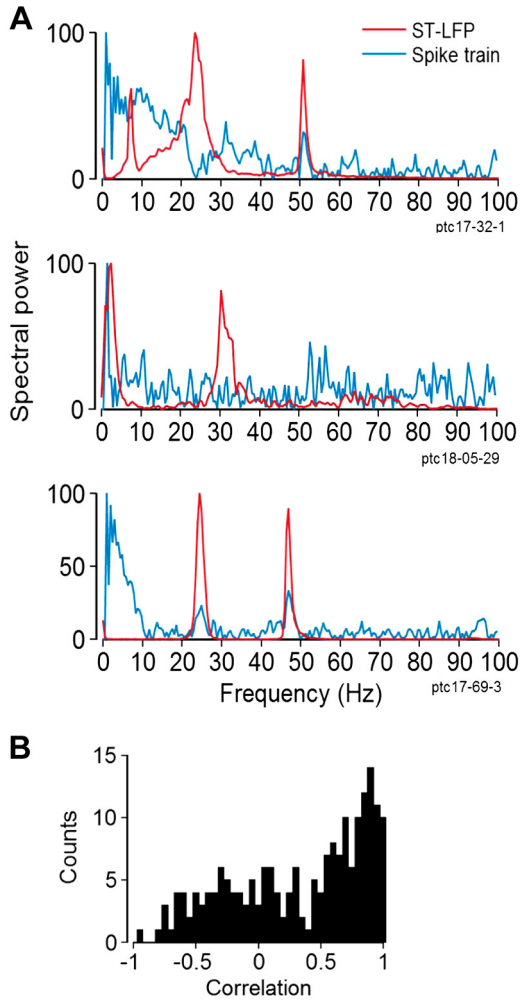

Fig. 7. *A*: 3 examples of comparisons of the spike-triggered local field potential (ST-LFP) spectrum (red lines) with the firing rate spectrum (blue lines) of the same units. *B*: the distribution of cross-correlations between peak shapes for all units with >1,000 spikes.

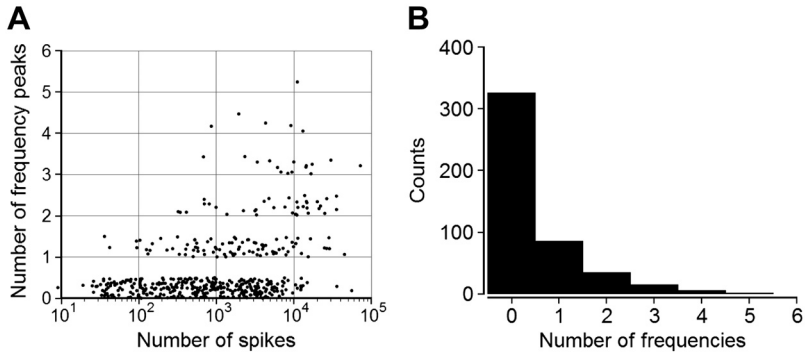

Fig. 8. Synchrony is more prevalent in higher-firing rate units. *A*: scatterplot showing relation between the total number of spikes fired by a unit during a recording (*x*-axis) and the number of unique frequency peaks in the spike-triggered local field potential spectrum (*y*-axis). Random scatter in the range 0–0.5 has been added to the *y*-axis values to better show the distribution across different units. *B*: histogram derived from the values in *A* showing the distribution of frequency numbers across units.

tended to fire when there was less than normal LFP energy present. The measure can be interpreted as a measure of the "driving effect" of LFP power, per se, on the firing of the cell. In principle the measure is independent of the correlation measure, although in practice the two were highly correlated. In neither case was there any obvious difference between groups. Overall, it seems unlikely that the variation in frequency specificity among cells is an artifact of strong positive or negative correlations between their firing rates and the amplitudes of particular frequencies on a timescale of several seconds. It is possible, however, that there is a systematic relationship on shorter timescales.

Random jitter of spike times reduces peak height predictably. We additionally tested the dependence of the ST-LFP signal on phase by randomly jittering spike times. Jitter will cause random changes in the phase values for each spike and hence should reduce the heights of peaks in the ST-LFP power spectrum if there is a systematic relation with phase. The amount of temporal jitter required to reduce peak height by a given amount should scale linearly with the period of the peak (i.e., the inverse of its frequency). If on the other hand there is no significant relationship between spike times and phase, jitter should have no consistent effect. We found that jitter consistently reduced the height of peaks in the ST-LFP. To quantify this, we jittered spike times by adding a random time value uniformly distributed in the interval $\pm t_j$ where t_j is the jitter value. We estimated the amount of jitter required to reduce the height of each peak to 10% of its value. This was done by calculating ST-LFP profiles for a set of 13 jitter values, logarithmically spaced between 5 and 320 ms, and interpolating to find the value at which height declined to 10% of the peak value. Figure 11 shows that the amount of jitter required to do this increased linearly (with the exception of 1 data point) as a function of peak period. An amount of jitter just under half the value of the period was sufficient. For the highest frequencies in the sample (~90 Hz), values of jitter ~4 ms were able to substantially reduce peak height, indicating extremely precise firing of spikes in relation to the LFP.

Units synchronize to phase-pair combinations. In cases where units synchronize to more than one frequency, we asked whether individual spikes tend to fire preferentially at specific phase combinations of the two frequencies or whether interactions are absent and the phase values are independent. To do this we calculated, as described in METHODS, histograms $J(i, j)$ of the distribution of phase angles, ϕ_1 and ϕ_2, with binned values i and j, respectively, of individual spikes, for pairs of frequency peaks identified in the ST-LFP spectrum. Bins were 18° wide. Control data were obtained by time-reversing the LFP signals.

We used χ^2-tests to make the following comparisons: *1*) the experimental distribution was compared with a random model in which there was no interaction with phase and the expected distribution was uniform; *2*) the time-reversed control was compared with a uniform distribution; *3*) the experimental distribution was compared with that obtained by adding the marginal distributions of phase angle (the sum model), as would be predicted in the case where half of the spikes fire randomly with respect to the phase of one of the two frequencies and the other half fires randomly with respect to the phase of the other frequency. This might happen, for example, if the frequencies rarely co-occurred in time, or possibly in the case of bad spike sorting where the spikes were a mixture of those from two units, each synchronized to a single frequency. (We did not test other hypothetical firing ratios, which would yield somewhat different models.) Finally, *4*) we compared the experimental distribution with that obtained by multiplying the marginal distributions (the product model), as would be expected if the probability of firing was the product of the individual firing probabilities, and hence interactive. A Bonferroni correction for multiple comparisons was not used, given that statistical test results were not used to select examples for evaluation; however, the effects of multiple compari-

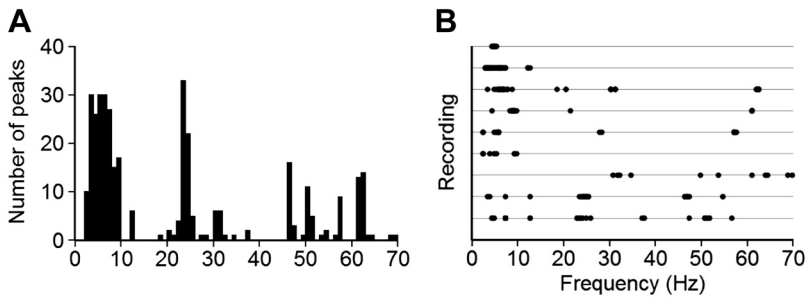

Fig. 9. Units synchronize to a wide range of frequencies. *A* shows the distribution of spike-triggered local field potential peak frequencies, and *B* breaks this down by recording (each horizontal line shows the values for a particular recording).

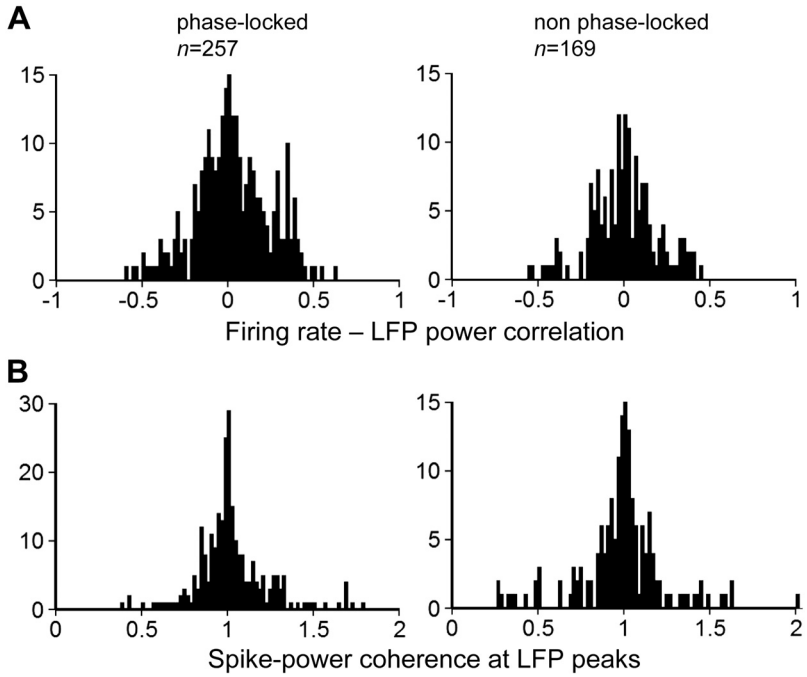

Fig. 10. Absence of synchrony to a local field potential (LFP) frequency is not due to units only firing at times when the frequency is absent. Histograms of values of the correlation between firing rate and spectral power as functions of time (*A*) and values of the spike-power coherence measure (*Eq. 6*) (*B*) for LFP frequency peaks to which a given unit was significantly phase-locked ($P < 0.001$, *left*) and for unit-peak pairs where there was no statistical evidence of phase-locking ($P > 0.5$, *right*). The distributions are similar for unit-peak pairs where there is phase-locking and pairs where there is not.

sons are considered in what follows. Figure 12 shows examples of joint phase distributions from frequency pairs in four different units, together with the time-reversed control and the distributions predicted by the sum and product models.

The hypothesis that phase values were random could be rejected at $P < 0.05$ for 66 of 69 frequency pairs. This is expected given that nonrandomness of phase values was used to identify frequency peaks in the first place. A control comparison, of histograms from the time-reversed LFP (examples shown in 2nd column of Fig. 12) with a uniform distribution, showed that in this case the random model could be rejected in only eight cases. Three or four of these cases (~1/20th of 69) might be expected to occur if the random model is correct, as is hypothetically true in this case. Comparison of the data with the sum model (examples in 3rd column of Fig. 12) showed that the sum model could be rejected for 50 of 69 pairs, i.e., neither the random nor the sum model was a good description of the data. In contrast, comparison of the product model (4th column of Fig. 12) with the data showed that the model could be rejected at $P < 0.05$ for only 9 of 69 pairs. At least three or four of these cases would be expected to occur, even if the product model was always correct. Hence it seems reasonable to conclude that in most cases there is good evidence that the firing of units is determined by phase combinations of frequency pairs. In no case was P(sum model) $>$ P(product model), although in four cases both models could be rejected. One of these is shown in Fig. 12*D*.

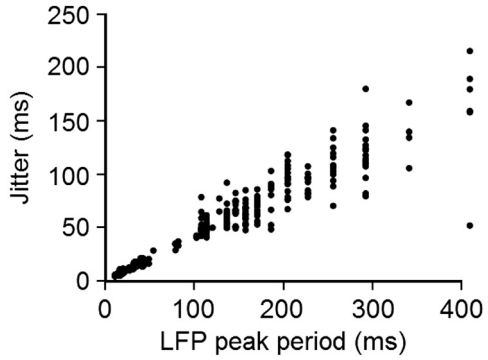

Fig. 11. Spike-time jitter reduces peak height in a predictable way. The amount of jitter required to reduce spike-triggered local field potential (LFP) peak height to 10% of its initial value is linearly related to the period (reciprocal of frequency) of the peak for all the unit-peak pairs in the sample.

Parameters obtained from fits of a von Mises model function to the joint phase histograms (see METHODS) showed that the width of the peak in the histogram (distance to half-height along the diagonal) was positively correlated with the lower frequency of a given frequency pair (Fig. 12*E*; $r = 0.5$, $P < 0.001$). That is, expressed in terms of phase, phase-locking was tighter for lower frequencies. This might imply an equivalent temporal scatter, however, in terms of actual time values. There was no correlation with the higher of the two frequencies (data not shown). There was no clear grouping, or correlation, of the phases at which particular units synchronized (Fig. 12*F*).

Units variably synchronize to the screen refresh rate. We analyzed six recordings of 16- to 20-min duration each from three different animals where the visual stimulus was a blank screen with a 66-Hz refresh rate and the LFP showed an oscillatory, desynchronized pattern. In all of these experiments a clear 66-Hz signal was present in the LFP. As with naturally occurring LFP frequencies, some units synchronized to this frequency but others did not. We tested this quantitatively by finding the smallest Rayleigh probability that the distribution of phase angles was random at a target frequency of 66 Hz taken over all 10 channels. A Bonferroni correction with $n = 10$ was applied. Out of a total of 157 units, 48 had (corrected) P values < 0.001, whereas 32 had (uncorrected) $P > 0.5$, indicating no detectable synchrony. Units that were synchronized did not seem distinguishable from those that were not in any obvious respect: firing rates were somewhat lower among the unsynchronized group (as with naturally occurring LFP frequencies: Fig. 8) but overlapped substantially, whereas the

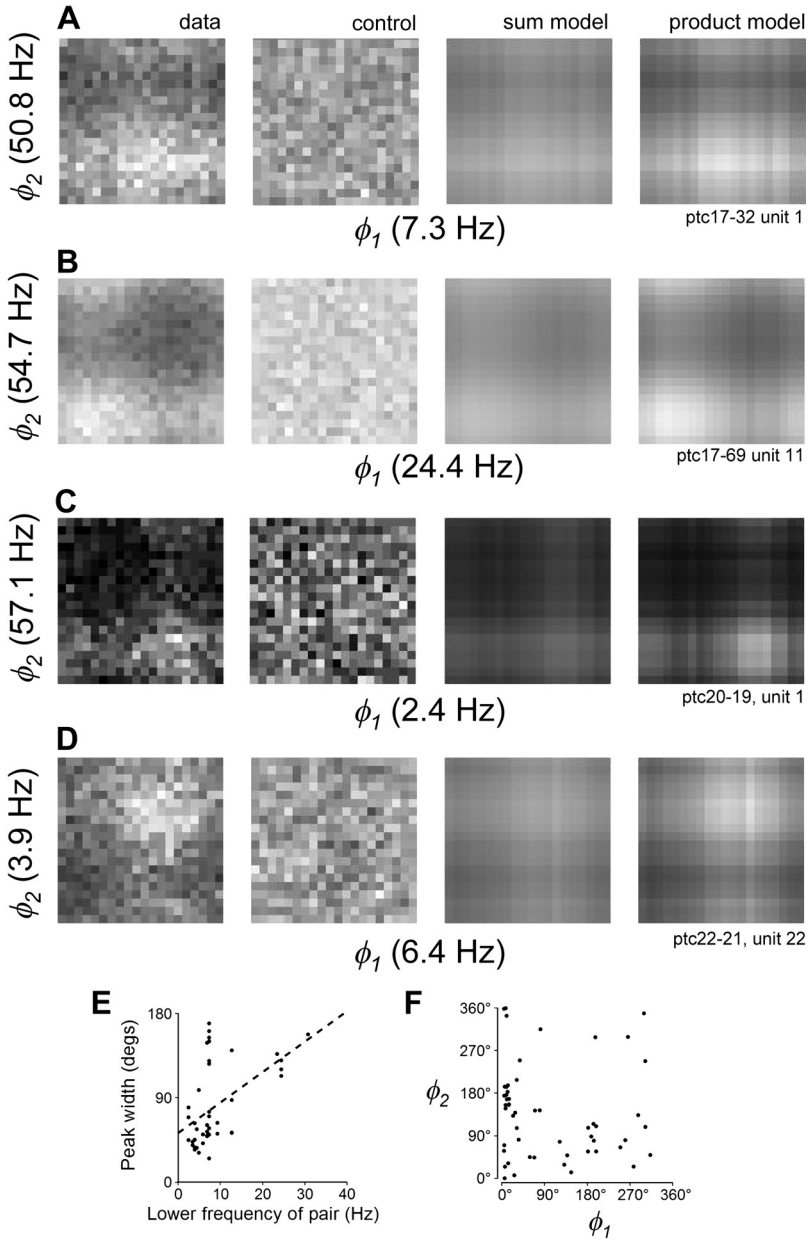

Fig. 12. Units often synchronize to phase combinations of frequency pairs. *A–D*: 2-dimensional histograms of the phase values (ϕ) (0–360° in 18° bins) for 2 different frequencies measured at times of spike occurrence. Data from 4 different units from different recordings (*A*, *B*, *C*, and *D*) are shown. "Data" panels show the experimentally measured distribution. "Control" panels show the distributions obtained from the same units after time-reversing the local field potential signal. "Sum model" panels show predicted distributions in the case that half of the spikes fire randomly to one phase and systematically to the other, and vice versa for the other half. "Product model" panels show the distribution expected if the probability of firing to a phase combination is the product of the probability of firing to each phase. Statistical tests comparing data with uniform distributions gave $P < 10^{-31}$ in all 4 cases; comparisons of time-reversed controls with a uniform distribution gave $P > 0.52$ for *A–C* and $P \sim 10^{-4}$ for *D*. Comparison of the data with the sum model gave $P < 10^{-4}$ in all 4 cases; comparison with the product model gave $P > 0.2$ for *A–C* and $P < 10^{-4}$ for *D*. *E*: the relationship between the lower frequency of a given pair and the width of the peak (distance to half-height along the diagonal) measured in degrees of phase angle. There is a significant positive correlation ($r = 0.5$, $P < 0.001$). *F*: the peak phase for the lower frequency vs. the peak phase for the higher frequency. See METHODS for further details.

distribution in depth along the electrode of both groups was similar. Both 66-Hz synchronized and unsynchronized units were often, though not always, synchronized to one or more other, nonartifactual frequencies in the LFP.

Synchrony is unlikely to be due to artifactual sources of LFP oscillation. We considered possible artifactual explanations for our findings. Oscillations in the recorded LFP can be induced by external electromagnetic fields (EMFs) as well as by luminance flicker at or below 100 Hz, which can synchronize the firing of neurons (Williams et al. 2004). EMFs are very unlikely to cause neurons to fire, unless extremely powerful, as in transcranial magnetic stimulation, although their signals can easily be picked up as a result of inefficient shielding and/or grounding. We frequently observed a 60-Hz signal in the LFP (e.g., Fig. 1), the frequency of the mains electricity supply in Canada. Although this could sometimes induce a weak 60-Hz peak in the ST-LFP spectrum, especially when obtained from only a small number (<500) of spikes, peaks at 60 Hz were never identified by the methods that took statistical significance into account. This and other artifactual, electronic, EMF sources would be expected to show constancy of frequency and phase over long time intervals, i.e., to exhibit coherence lengths of seconds or more. We measured the phase coherence of the ST-LFP frequency peaks by plotting the amplitude of the peak as a function of spike train shift, for a range of shifts between –2.0 and +2.0 s. A Gaussian was fitted to these values, and the width, σ_s, measured. A shift of this value can be expected to reduce the height of the ST-LFP peak to ~61%. Note that shifting the spike train shifts the ST-LFP waveform within the window used for the calculation of the power spectrum, which was ~2 s. Because of this, the method will fail to measure coherence lengths much shorter than the temporal window. Longer coherence lengths can be measured, however, and if present might suggest the presence of artifactual signals.

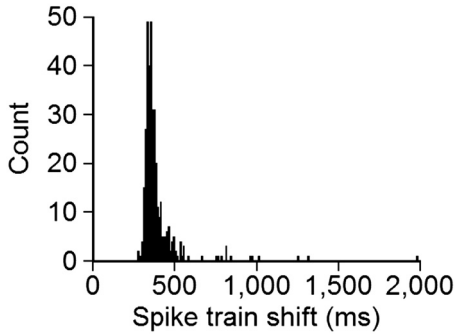

Fig. 13. Spike train shift reduces the heights of spike-triggered local field potential (ST-LFP) spectral peaks, indicating limited temporal coherence of oscillatory signals. The histogram shows the amount of spike train shift required to reduce the amplitude of peaks in the ST-LFP spectrum by ~61%, i.e., the value of σ_s. See text for further description.

Figure 13 shows the distribution of values of σ_s for all the significant unit-frequency peaks in our data. Nearly all the points have values $<$ 500 ms, demonstrating that coherence lengths were normally always shorter than the temporal window used for the calculation of the ST-LFP spectrum. We also applied this test to the recordings made with a 66-Hz monitor refresh rate. In these the ST-LFP spectral peaks for 66-Hz signals, as expected, did not decline appreciably up to the largest shifts tested ($\pm$20 s).

DISCUSSION

Significance of the desynchronized periods. The periods of oscillatory, desynchronized LFP activity we observed may be similar to the fast oscillations observed under ketamine-xylazine anesthesia by Steriade and Amzica (1996). It is possible that cats undergo periods of REM sleep under anesthesia and that the LFP changes accordingly to a desynchronized state. Similar state changes were observed in anesthetized rats (Clement et al. 2008) and identified as REM sleep because of accompanying physiological changes including increased heart and respiration rates that are characteristic of REM sleep. Sudden increases in heart rate accompanying switches from synchronized to desynchronized activity were also seen previously in N. V. Swindale's laboratory in experiments on cats in which both EEG spectrum and heart rate were continuously recorded (unpublished data). Cats, as predators, spend ~25% of total sleep time in REM sleep, with durations of episodes up to 20 min (Jouvet 1967). The frequency and duration of desynchronized episodes we observed are consistent with these observations. One reason why they may not have been reported more commonly before is that it is a normal practice to administer atropine, a long-lasting muscarinic blocker, before induction of anesthesia. Atropine suppresses REM sleep (Shiromani et al. 1987). Clement et al. (2008) likewise observed that the desynchronized periods in anesthetized rats were abolished by atropine. Stimulation of the basal forebrain, a source of cholinergic inputs to the cortex, is known to induce a desynchronized state in visual cortex (Duque et al. 2000; Goard and Dan 2009; Pinto et al. 2013), and it is possible that atropine blocks REM sleep by acting on this pathway.

Our experimental records showed that systemic atropine was not used as a preanesthetic agent in those animals that showed the most prominent periods of oscillatory LFP activity, although further observations would be required to confirm this link. Although we did not use atropine as a preanesthetic agent, other drugs including xylazine (an α_2-adrenergic receptor agonist) and buprenorphine (a μ-opioid receptor agonist) were given. These drugs might have predisposed the brain to oscillatory states, although the mechanism(s) by which this might happen is unclear. Overall, our observations, and those of Clement et al. (2008), strengthen the analogy between anesthesia and sleep (Tung and Mendelson 2004).

If our desynchronized states are REM states, they may be different from the desynchronized states observed in other experiments (e.g., Goard and Dan 2009; Marguet and Harris 2011) and that in anesthetized animals are often produced by basal forebrain or sensory stimulation. Desynchronized states in awake animals are normally associated with alertness and focused attention (Berger 1929; Harris and Thiele 2011). Such states, although superficially similar to REM states in terms of EEG pattern, would be expected to be different functionally. Although the functions of REM sleep remain unclear, involvement in the recall of stored memories has been suggested (Crick and Mitchison 1983). Given the association of REM sleep with dreaming, it might not be surprising if during it the brain engaged in patterns of activity that reflected the use of internal codes and signaling mechanisms that were different from those involved in processing sensory stimuli during alertness.

Whatever the significance of these states, neural behavior during them is extremely distinctive, with synchrony between neural spiking and multiple frequency components of the LFP as well as locking to specific phase relations between frequency pairs. The frequencies with which these patterns of synchrony occurred covered a wide range (Fig. 9) and included 2–10 Hz (theta), 20–35 Hz (beta), and 45–70 Hz (gamma). There are a number of reasons why similar observations might not have been made before. As suggested above, the states in which they occur may normally be suppressed during recordings from anesthetized animals because of the use of atropine. Our observations also required analysis of relatively long ($>$15 min) periods of activity and averaging over hundreds of spikes to show clear signals. Such recordings are generally not made in experiments on anesthetized visual cortex when the main goal is to measure responses to visual stimuli. Oscillatory frequencies were often of low amplitude and only visible when displayed using logarithmic power scaling (e.g., Fig. 1).

Relation to prior observations of spike-LFP synchrony. In non-REM states, synchrony of spikes to LFP oscillations (often stimulus induced) has been reported in a variety of species and brain regions, including the awake rat hippocampus (O'Keefe and Recce 1993); awake monkey V4 (Fries et al. 2001), area LIP (Pesaran et al. 2002), somatosensory cortex (Ray et al. 2008), and sensorimotor cortex (Murthy and Fetz 1992); and cat visual cortex (Eckhorn et al. 1988; Gray and Singer 1989). Phase-locking of units to an oscillation frequency in the LFP is perhaps unremarkable in itself given that the LFP must reflect local spiking activity (or synaptic inputs causing spiking) and hence almost by definition phase-locking must be present. It is perhaps more surprising to find highly selective frequency synchronization to more than one frequency in individual cells together with variable patterns of synchrony among neighboring cells. However, earlier studies have provided signs of such variability. Differences among multiunits in spike-LFP cou-

pling were noted by Destexhe et al. (1999; their Fig. 6*C*), although these did not specifically relate to frequency. Williams et al. (2004) noted that not all neurons in anesthetized macaque monkey V1 synchronized to 60-Hz or 100-Hz frame rate modulation of an optimal visual stimulus, although a much higher proportion of them did (up to 82%) than in the present study. Some of this difference might be attributed to the fact that Williams et al. used visual stimuli to drive cells. Had they recorded responses to a flickering blank screen, lower levels of synchrony might have been found. Most relevant to the present findings is a study by Nuñez et al. (1992) in which intracellular recordings were made from neurons in motor and association cortex in urethane-anesthetized cats. Among these neurons a small number were found that exhibited subthreshold membrane oscillations in response to injected DC current. In at least one case (Fig. 2*B* of Nuñez et al. 1992), a neuron exhibited simultaneous narrow-band oscillations of membrane potential at harmonically unrelated frequencies of 19, 30, and 39 Hz.

Origins of the oscillations. The variability among units that we observed might reflect variability intrinsic to the cell, the existence of multiple local subnetworks of neurons with different oscillatory properties, or the presence of varied oscillatory inputs to the cortex from distant structures. Considering each of these possibilities in turn, there is evidence that individual hippocampal neurons (García-Muñoz et al. 1993; Leung and Yim 1991; Núñez et al. 1987) and neocortical neurons (Dwyer et al. 2012; Gutfreund et al. 1995; Hutcheon and Yarom 2000) have resonance properties based on membrane characteristics. However, the available evidence suggests that the resonance frequencies are too low (<20 Hz) and broad to account for our observations, nor do we know of evidence that cells show membrane-based resonance to multiple frequencies. Models of coupled networks of cells can display narrow-band resonance to temporally modulated inputs (Kang et al. 2010) including resonance to two frequencies (Ledoux and Brunel 2011), and it is possible that intrinsic membrane resonance might contribute to these properties (Moca et al. 2014). The finding that some units have peaks in their firing rate spectrograms that coincide with peaks in the ST-LFP spectrum (Fig. 7*A*) is consistent with the possibility that the oscillations are a local network property (Buzsáki and Draguhn 2004; Wang 2010). One cannot be certain of this, however, because an external oscillatory source might modulate the unit's firing strongly enough that it would fire spikes at temporal intervals matching the oscillatory frequency. In addition, about half of the unit-frequency peak pairs in our sample did not show any reliable evidence of oscillatory activity in their firing at the phase-locking frequency (Fig. 7*A*).

An alternative to cell- or local subnetwork-specific frequency selectivity is that unit firing is modulated by inputs that come from outside the visual cortex. Particular cells might selectively connect with specific sets of inputs, each with a characteristic oscillation frequency. LFP signals would reflect oscillating subthreshold currents produced by these inputs. Cortical cells would then act as filters, firing at coincident phases of the inputs as shown in Fig. 12. The effect of the oscillatory inputs would be to modulate the timing of spikes rather than producing them. This behavior would also be consistent with our finding that cells' firing rates are variably, and sometimes negatively, correlated with the amplitudes of the frequencies of the LFP components with which their spikes are synchronized (Fig. 10). The absence of spectral peaks, or gaps in the spectrum, at synchronizing frequencies might be the result of cells synchronizing their spikes to phase alignments of different frequencies (Fig. 12). This could lead to a loss of intervals between spikes matching either of the two frequencies.

Additional reasons for lack of synchrony between particular units and frequencies are as follows. Although there is a lack of obvious covariation between spectral amplitude and firing rate on a timescale of several seconds, it is nevertheless possible that on a timescale of seconds or less nonsynchronizing units do not fire spikes during short frequency bursts. This, however, could not explain the lack of synchrony of some units to the artifactual 66-Hz stimulus, since that was constantly present. It is also possible that some units might synchronize to both positive and negative phases of an LFP frequency, leading to a cancellation in the linear summation that underlies the calculation of the ST-LFP waveform.

Functional roles for selective phase-locking. Oscillations have been thought to underlie a variety of possible functions related to stimulus coding by the nervous system, including phase coding of stimuli or multiplexing sensory information streams within single neurons or populations of neurons to selectively address different targets (Akam and Kullmann 2014; Panzeri et al. 2010). Our observations come from periods of spontaneous activity and so do not directly address issues of stimulus coding. However, assuming that the function of neuronal activity in REM sleep (or whatever mechanisms were generating the neural activity seen in our experiments) is not meaningless, and given the ability of the brain to produce meaningful patterns of activity in the absence of sensory stimulation, it is not unlikely that visual cortex neurons might be involved in the recall of visual memories. This might involve the selective addressing of neurons by inputs with a frequency combination code, perhaps with the result of evoking spikes occurring at defined times with respect to the inputs. Given the results shown in Fig. 11, the timing might be as precise as 4 ms for the higher frequencies in our sample. This mechanism might involve all the factors discussed above: intrinsic membrane and network properties leading to selective and variable resonances in networks of cortical neurons, which would allow individual neurons to respond selectively to oscillatory signals from external inputs. The responses would code for the evoked memories. Behavior of this nature is required by content-addressable memories that have to respond quickly in information-rich ways to different inputs (Swindale 2008). Another point of view is that all brains have the task of producing complex spatio-temporal patterns of neural activity (ultimately to become motor activity) in which temporal patterns have to be planned in advance (Yuste et al. 2005). One way of doing this might be to use frequency combinations that have the property that they will result in the generation of spikes at defined future times subsequent to the initiation of the oscillations. Hence oscillatory combination codes might underlie planned movements.

Neuronal variability. This study has identified temporal properties that vary between neurons. Reasons for the variability might ultimately involve factors determined by the variable genetic expression of cortical neurons (Tasic et al. 2016; Zeisel et al. 2015), including the channel types that determine temporal membrane and biophysical properties, the molecules that

determine connections with other neurons, and the characteristics of released transmitters. Hence the findings of this study may provide a link between the genetic variability of cortical neurons and functionally important frequency-related behaviors that are more complex than those of the conventional receptive field properties of V1 neurons.

ACKNOWLEDGMENTS

We thank Lawrence Ward and Catalin Mitelut for helpful comments.

GRANTS

This work was supported by grants from the Canadian Institutes of Health Research and the Natural Sciences and Engineering Research Council of Canada.

DISCLOSURES

No conflicts of interest, financial or otherwise, are declared by the authors.

AUTHOR CONTRIBUTIONS

N.V.S. and M.A.S. conceived and designed research; N.V.S. and M.A.S. performed experiments; N.V.S. analyzed data; N.V.S. interpreted results of experiments; N.V.S. prepared figures; N.V.S. drafted manuscript; N.V.S. and M.A.S. edited and revised manuscript; N.V.S. and M.A.S. approved final version of manuscript.

REFERENCES

Akam T, Kullmann DM. Oscillatory multiplexing of population codes for selective communication in the mammalian brain. *Nat Rev Neurosci* 15: 111–122, 2014. doi:10.1038/nrn3668.

Ascoli GA, Alonso-Nanclares L, Anderson SA, Barrionuevo G, Benavides-Piccione R, Burkhalter A, Buzsáki G, Cauli B, Defelipe J, Fairén A, Feldmeyer D, Fishell G, Fregnac Y, Freund TF, Gardner D, Gardner EP, Goldberg JH, Helmstaedter M, Hestrin S, Karube F, Kisvárday ZF, Lambolez B, Lewis DA, Marin O, Markram H, Muñoz A, Packer A, Petersen CC, Rockland KS, Rossier J, Rudy B, Somogyi P, Staiger JF, Tamas G, Thomson AM, Toledo-Rodriguez M, Wang Y, West DC, Yuste R; Petilla Interneuron Nomenclature Group. Petilla terminology: nomenclature of features of GABAergic interneurons of the cerebral cortex. *Nat Rev Neurosci* 9: 557–568, 2008. doi:10.1038/nrn2402.

Barthó P, Hirase H, Monconduit L, Zugaro M, Harris KD, Buzsáki G. Characterization of neocortical principal cells and interneurons by network interactions and extracellular features. *J Neurophysiol* 92: 600–608, 2004. doi:10.1152/jn.01170.2003.

Batschelet E. *Circular Statistics in Biology*. London: Academic, 1981.

Berger H. Über das Elektroenkephalogramm des Menschen. *Arch Psychiatr Nervenkr* 87: 527–570, 1929. doi:10.1007/BF01797193.

Blanche TJ, Spacek MA, Hetke JF, Swindale NV. Polytrodes: high-density silicon electrode arrays for large-scale multiunit recording. *J Neurophysiol* 93: 2987–3000, 2005. doi:10.1152/jn.01023.2004.

Buzsáki G, Draguhn A. Neuronal oscillations in cortical networks. *Science* 304: 1926–1929, 2004. doi:10.1126/science.1099745.

Clement EA, Richard A, Thwaites M, Ailon J, Peters S, Dickson CT. Cyclic and sleep-like spontaneous alternations of brain state under urethane anaesthesia. *PLoS One* 3: e2004, 2008. doi:10.1371/journal.pone.0002004.

Crick F, Mitchison G. The function of dream sleep. *Nature* 304: 111–114, 1983. doi:10.1038/304111a0.

Destexhe A, Contreras D, Steriade M. Spatiotemporal analysis of local field potentials and unit discharges in cat cerebral cortex during natural wake and sleep states. *J Neurosci* 19: 4595–4608, 1999. doi:10.1523/JNEUROSCI.19-11-04595.1999.

Duque A, Balatoni B, Detari L, Zaborszky L. EEG correlation of the discharge properties of identified neurons in the basal forebrain. *J Neurophysiol* 84: 1627–1635, 2000. doi:10.1152/jn.2000.84.3.1627.

Dwyer J, Lee H, Martell A, van Drongelen W. Resonance in neocortical neurons and networks. *Eur J Neurosci* 36: 3698–3708, 2012. doi:10.1111/ejn.12001.

Eckhorn R, Bauer R, Jordan W, Brosch M, Kruse W, Munk M, Reitboeck HJ. Coherent oscillations: a mechanism of feature linking in the visual cortex? Multiple electrode and correlation analyses in the cat. *Biol Cybern* 60: 121–130, 1988. doi:10.1007/BF00202899.

Fisher NI. *Statistical Analysis of Circular Data*. Cambridge, UK: Cambridge Univ. Press, 1993.

Fries P, Reynolds JH, Rorie AE, Desimone R. Modulation of oscillatory neuronal synchronization by selective visual attention. *Science* 291: 1560–1563, 2001. doi:10.1126/science.1055465.

García-Muñoz A, Barrio LC, Buño W. Membrane potential oscillations in CA1 hippocampal pyramidal neurons in vitro: intrinsic rhythms and fluctuations entrained by sinusoidal injected current. *Exp Brain Res* 97: 325–333, 1993. doi:10.1007/BF00228702.

Goard M, Dan Y. Basal forebrain activation enhances cortical coding of natural scenes. *Nat Neurosci* 12: 1444–1449, 2009. doi:10.1038/nn.2402.

Gray CM, Singer W. Stimulus-specific neuronal oscillations in orientation columns of cat visual cortex. *Proc Natl Acad Sci USA* 86: 1698–1702, 1989. doi:10.1073/pnas.86.5.1698.

Gutfreund Y, Yarom Y, Segev I. Subthreshold oscillations and resonant frequency in guinea-pig cortical neurons: physiology and modelling. *J Physiol* 483: 621–640, 1995. doi:10.1113/jphysiol.1995.sp020611.

Harris KD, Thiele A. Cortical state and attention. *Nat Rev Neurosci* 12: 509–523, 2011. doi:10.1038/nrn3084.

Hubel DH, Wiesel TN. Receptive fields, binocular interaction and functional architecture in the cat's visual cortex. *J Physiol* 160: 106–154, 1962. doi:10.1113/jphysiol.1962.sp006837.

Hutcheon B, Yarom Y. Resonance, oscillation and the intrinsic frequency preferences of neurons. *Trends Neurosci* 23: 216–222, 2000. doi:10.1016/S0166-2236(00)01547-2.

Jeans J. *An Introduction to the Kinetic Theory of Gases*. Cambridge, UK: Cambridge Univ. Press, 1967.

Jouvet M. Neurophysiology of the states of sleep. *Physiol Rev* 47: 117–177, 1967. doi:10.1152/physrev.1967.47.2.117.

Kang K, Shelley M, Henrie JA, Shapley R. LFP spectral peaks in V1 cortex: network resonance and cortico-cortical feedback. *J Comput Neurosci* 29: 495–507, 2010. doi:10.1007/s10827-009-0190-2.

Kubota Y. Untangling GABAergic wiring in the cortical microcircuit. *Curr Opin Neurobiol* 26: 7–14, 2014. doi:10.1016/j.conb.2013.10.003.

Ledoux E, Brunel N. Dynamics of networks of excitatory and inhibitory neurons in response to time-dependent inputs. *Front Comput Neurosci* 5: 25, 2011. doi:10.3389/fncom.2011.00025.

Leung LW, Yim CY. Intrinsic membrane potential oscillations in hippocampal neurons in vitro. *Brain Res* 553: 261–274, 1991. doi:10.1016/0006-8993(91)90834-I.

Marguet SL, Harris KD. State-dependent representation of amplitude-modulated noise stimuli in rat auditory cortex. *J Neurosci* 31: 6414–6420, 2011. doi:10.1523/JNEUROSCI.5773-10.2011.

Moca VV, Nikolic D, Singer W, Mureşan RC. Membrane resonance enables stable and robust gamma oscillations. *Cereb Cortex* 24: 119–142, 2014. doi:10.1093/cercor/bhs293.

Murthy VN, Fetz EE. Coherent 25- to 35-Hz oscillations in the sensorimotor cortex of awake behaving monkeys. *Proc Natl Acad Sci USA* 89: 5670–5674, 1992. doi:10.1073/pnas.89.12.5670.

Nauhaus I, Busse L, Carandini M, Ringach DL. Stimulus contrast modulates functional connectivity in visual cortex. *Nat Neurosci* 12: 70–76, 2009. doi:10.1038/nn.2232.

Nowak LG, Azouz R, Sanchez-Vives MV, Gray CM, McCormick DA. Electrophysiological classes of cat primary visual cortical neurons in vivo as revealed by quantitative analyses. *J Neurophysiol* 89: 1541–1566, 2003. doi:10.1152/jn.00580.2002.

Nuñez A, Amzica F, Steriade M. Voltage-dependent fast (20–40 Hz) oscillations in long-axoned neocortical neurons. *Neuroscience* 51: 7–10, 1992. doi:10.1016/0306-4522(92)90464-D.

Núñez A, García-Austt E, Buño W Jr. Intracellular theta-rhythm generation in identified hippocampal pyramids. *Brain Res* 416: 289–300, 1987. doi:10.1016/0006-8993(87)90909-7.

O'Keefe J, Recce ML. Phase relationship between hippocampal place units and the EEG theta rhythm. *Hippocampus* 3: 317–330, 1993. doi:10.1002/hipo.450030307.

Panzeri S, Brunel N, Logothetis NK, Kayser C. Sensory neural codes using multiplexed temporal scales. *Trends Neurosci* 33: 111–120, 2010. doi:10.1016/j.tins.2009.12.001.

Pesaran B, Pezaris JS, Sahani M, Mitra PP, Andersen RA. Temporal structure in neuronal activity during working memory in macaque parietal cortex. *Nat Neurosci* 5: 805–811, 2002. doi:10.1038/nn890.

Pinto L, Goard MJ, Estandian D, Xu M, Kwan AC, Lee SH, Harrison TC, Feng G, Dan Y. Fast modulation of visual perception by basal forebrain cholinergic neurons. *Nat Neurosci* 16: 1857–1863, 2013. doi:10.1038/nn.3552.

Press WH, Teukolsky SA, Vetterling WT, Flannery BP. *Numerical Recipes: The Art of Scientific Computing* (2nd ed.). Cambridge, UK: Cambridge Univ. Press, 1994.

Ray S, Hsiao SS, Crone NE, Franaszczuk PJ, Niebur E. Effect of stimulus intensity on the spike-local field potential relationship in the secondary somatosensory cortex. *J Neurosci* 28: 7334–7343, 2008. doi:10.1523/JNEUROSCI.1588-08.2008.

Shiromani PJ, Gillin JC, Henriksen SJ. Acetylcholine and the regulation of REM sleep: basic mechanisms and clinical implications for affective illness and narcolepsy. *Annu Rev Pharmacol Toxicol* 27: 137–156, 1987. doi:10.1146/annurev.pa.27.040187.001033.

Spacek MA, Swindale NV. Cortical state and natural movie responses in the cat visual cortex (Preprint). *bioRxiv* 031765, 2016. doi:10.1101/031765.

Steriade M, Amzica F. Intracortical and corticothalamic coherency of fast spontaneous oscillations. *Proc Natl Acad Sci USA* 93: 2533–2538, 1996. doi:10.1073/pnas.93.6.2533.

Stevens CF. Neuronal diversity: too many cell types for comfort? *Curr Biol* 8: R708–R710, 1998. doi:10.1016/S0960-9822(98)70454-3.

Swindale NV. Feedback decoding of spatially structured population activity in cortical maps. *Neural Comput* 20: 176–204, 2008. doi:10.1162/neco.2008.20.1.176.

Swindale NV, Spacek MA. Spike sorting for polytrodes: a divide and conquer approach. *Front Syst Neurosci* 8: 6, 2014. doi:10.3389/fnsys.2014.00006.

Tasic B, Menon V, Nguyen TN, Kim TK, Jarsky T, Yao Z, Levi B, Gray LT, Sorensen SA, Dolbeare T, Bertagnolli D, Goldy J, Shapovalova N, Parry S, Lee C, Smith K, Bernard A, Madisen L, Sunkin SM, Hawrylycz M, Koch C, Zeng H. Adult mouse cortical cell taxonomy revealed by single cell transcriptomics. *Nat Neurosci* 19: 335–346, 2016. doi:10.1038/nn.4216.

Tung A, Mendelson WB. Anesthesia and sleep. *Sleep Med Rev* 8: 213–225, 2004. doi:10.1016/j.smrv.2004.01.003.

Wang XJ. Neurophysiological and computational principles of cortical rhythms in cognition. *Physiol Rev* 90: 1195–1268, 2010. doi:10.1152/physrev.00035.2008.

Williams PE, Mechler F, Gordon J, Shapley R, Hawken MJ. Entrainment to video displays in primary visual cortex of macaque and humans. *J Neurosci* 24: 8278–8288, 2004. doi:10.1523/JNEUROSCI.2716-04.2004.

Yuste R, MacLean JN, Smith J, Lansner A. The cortex as a central pattern generator. *Nat Rev Neurosci* 6: 477–483, 2005. doi:10.1038/nrn1686.

Zeisel A, Muñoz-Manchado AB, Codeluppi S, Lönnerberg P, La Manno G, Juréus A, Marques S, Munguba H, He L, Betsholtz C, Rolny C, Castelo-Branco G, Hjerling-Leffler J, Linnarsson S. Cell types in the mouse cortex and hippocampus revealed by single-cell RNA-seq. *Science* 347: 1138–1142, 2015. doi:10.1126/science.aaa1934.